Heliyon 10 (2024) e37979

Contents lists available at ScienceDirect

Heliyon

journal homepage: www.cell.com/heliyon

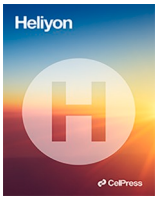

Research article

Systematic analysis of constitutive models of brain tissue materials based on compression tests

Wei Kang [a,b], Qiao Li [a], Lizhen Wang [a,b,*], Yu Zhang [a], Peng Xu [a], Yubo Fan [a,**]

[a] Key Laboratory of Biomechanics and Mechanobiology of Ministry of Education, Beijing Advanced Innovation Center for Biomedical Engineering, School of Biological Science and Medical Engineering, Beihang University, Beijing, 100083, China
[b] Innovation Center for Medical Engineering &Engineering Medicine, Hangzhou International Innovation Institute, Beihang University, 311115, Hangzhou, China

ARTICLE INFO

Keywords:
Brain tissue
Biomechanics
Compression test
Constitutive model

ABSTRACT

It's crucial to understand the biomechanical properties of brain tissue to comprehend the potential mechanisms of traumatic brain injury. This study, distinct from homogeneous models, integrates axonal coupling in both axial and transverse compressive experiments within a continuum mechanics framework to capture its intricate mechanical behaviors. Fresh porcine brains underwent unconfined compression at strain rates of 0.001/s and 0.1/s to 0.3 strain, allowing for a comprehensive statistical analysis of the directional, regional, and strain-rate-dependent mechanical properties of brain tissue. The established constitutive model, fitted to experimental data, delineates material parameters providing intuitive insights into the stiffness of gray/white matter isotropic matrices and neural fibers. Additionally, it predicts the mechanical performance of white matter matrix and axonal fibers under compressive loading. Results reveal that gray matter is insensitive to loading direction, exhibiting insignificant stiffness variations within regions. White matter, however, displays no significant differences in mechanical properties under axial and transverse loading, with an overall higher average stress than gray matter and a more pronounced strain-rate effect. Stress-strain curves indicate that, under axial compression, white matter axons primarily resist the load before transitioning to a matrix-dominated response. Under transverse loading, axonal fibers exhibit weaker resistance to lateral pressure. The mechanical behavior of brain tissue is highly dependent on loading rate, region, direction, and peak strain. This study, by combining experimentation with phenomenological modeling, elucidates certain phenomena, contributing valuable insights for the development of precise computational models.

1. Introduction

The brain is a highly complex organ containing sub-structures (brainstem, cerebellum, and cerebrum) and it is the most vulnerable biological soft tissue to external loading forces. Sudden external stresses and strains (tensile, compressive, and shear) caused by blunt force and transient acceleration exceeding a certain limit can cause traumatic brain injury (TBI), and to study the injury mechanism and protective equipment, finite element models of the head have been widely used to describe the biomechanical response of brain

* Corresponding author. Key Laboratory of Biomechanics and Mechanobiology of Ministry of Education, Beijing Advanced Innovation Center for Biomedical Engineering, School of Biological Science and Medical Engineering, Beihang University, Beijing, 100083, China.
** Corresponding author.
E-mail addresses: lizhenwang@buaa.edu.cn (L. Wang), yubofan@buaa.edu.cn (Y. Fan).

https://doi.org/10.1016/j.heliyon.2024.e37979
Received 17 June 2023; Received in revised form 27 August 2024; Accepted 14 September 2024
Available online 16 September 2024

tissue. However, high-fidelity computational models require accurate experimental data and precise constitutive equations.

The brain, as the softest tissue among all mammals, has highly nonlinear, anisotropic, and viscoelastic characteristics [1–5]. Measuring its mechanical properties is highly challenging, but macroscopic mechanical testing of the human brain has been carried out. Chatelin demonstrated that the brainstem is the stiffest region and adult brain tissue is relatively stiffer than that of children [6]. Some scholars have focused on the brain and indicated that white matter has a significant directional dependence [7,8], but Budday believes that brain tissue has not very obvious anisotropic mechanical properties [9]. Research on human brain tissue is also subject to strict ethical and regulatory constraints. Porcine brain tissue is often used as a substitute due to its anatomical, developmental, and growth similarities to the human brain, as well as its ease of access. It can be tested shortly after death, reducing the impact of tissue degradation on mechanical properties. Many scholars have conducted mechanical loading tests on porcine brains [7,10–12], bovine brains [13–15], and sheep brains [16,17] with similar structures, indicating a significant directional trend in white matter and regional dependence of brain tissue, which is reflected in sensitivity to load direction, velocity, and size. However, compression tests have shown that the strength of most regions in the cerebrum does not show significant differences in the absence of directional dependence by Li et al. [18]. Microscopic experiments such as indentation have the advantage of being lenient in sample requirements, only requiring a small portion of the tissue to be uniform. Some scholars have suggested that white matter is stiffer than gray matter through indentation experiments [19–21], while Elkin et al. believe that the cortex is stiffer than the brainstem, cerebellum, and corpus callosum [22]. Chen et al. refuted the mainstream view of regional homogeneity, stating that the internal corona radiata is also heterogeneous in the same region [23]. Jamal et al. used higher resolution and precision atomic force microscopy indentation to suggest that the mechanics of white matter depend on the orientation of axons [24]. Recently, magnetic resonance elastography has also been widely used, advancing the advantage of non-invasive in vivo assessment in its native environment [25–28]. The high heterogeneity of brain tissue makes it difficult to reach a unified conclusion from previous studies with different testing methods.

To describe the material properties of the brain using experimental data, an accurate constitutive model is required to establish the relationship between mechanical behavior and mechanical characteristics. Calibrated and validated constitutive models are crucial for simulating mechanical stimuli in brain tissue. To simulate the time-independent pseudoelastic behavior of brain tissue, material characterization is achieved through strain energy functions, expressed in terms of the invariants I_1, I_2, and I_3 of the right Cauchy-Green deformation tensor C. It is commonly assumed that brain tissue is incompressible, i.e., $I_3 = 1$. Mihai qualitatively and quantitatively captures the mechanical behavior of soft tissues within the framework of finite elasticity, indicating that Fung and Gent models, typically used for simulating soft tissues, are not suitable for modeling super-soft tissues like the brain under combined tension and shear [29,30]. Micro-mechanical models in hyperelastic methods are based on the microscopic structure and internal mechanisms of materials, modeling brain tissue's mechanical behavior by considering interactions at the atomic, molecular, or particle level. Kaster used the Arruda-Boyce model to describe the material behavior of brain tissue during indentation processes [31]. However, the stretching of chains can only be represented by the first invariant, which is less effective than phenomenological models based on experimental data and observed phenomena.

Due to the mismatch between microstructural models and soft tissue structures in hyperelastic models, compared to the assumption of isotropy in gray matter, brain white matter is assumed to have mechanical anisotropy due to the presence of axonal fibers and myelin sheaths. Strike a balance between accuracy, available data, and computational costs. Some scholars model white matter microstructures to capture regional material heterogeneity in brain tissue and establish microstructure models that can be applied to microscopic mechanical analysis of brain tissue to better understand diffuse axonal injuries. Pelegri's team has been studying fiber-reinforced composites (RAFCs) for years, identifying and generating representative volume element (RVE) micro-geometry structures for finite element analysis. The effective properties obtained from RVE represent the true properties of the material at the macroscopic scale, i.e., the smallest volume unit of material in composite materials used to represent the average constitutive response [32]. Based on this concept, Pan et al. first extended this concept to brain white matter, applying transition kinematic models to micro-mechanical finite element models to simulate axonal behavior in white matter tissues subjected to uniaxial tension [33]. However, the simplified model cannot effectively represent the widespread distribution of axonal distortion. They further used a stochastic process to establish pseudo three-dimensional representative volume elements (RVEs) similar to axonal structures in central nervous system white matter, embedded in the extracellular matrix (ECM) to study the mechanical response of white matter tissue at the tissue level [34]. Similarly, Wu et al. combined different volume fractions of axons and neuroglial cells to construct RVEs, calculated orthogonal anisotropic storage and loss moduli by frequency loading, and simulated the anisotropic viscoelasticity of white matter, used to explain the measurement results of MRE or other experimental modes [35,36]. The characteristics of axons and glial cells are taken from previous published works and literature. Agarwal et al. considered a hyperelastic model-based approach and appropriately cited spring-dashpot structured models to represent the connections between oligodendrocytes and axons, comparing the single-oligodendrocyte and multi-oligodendrocyte models to predict the accumulation of axonal injury and the risk of repeated loading damage [37,38]. They described axons and ECM matrices by obtaining the characteristics of axons and glial cells, respectively, using a nonlinear Ogden hyperelastic model, constructed RVEs, and simulated simple shear and pure shear to reproduce the Poynting Effect of white matter [39]. Karami et al. conducted a series of pioneering work to characterize the microstructure and uniform mechanical response of brain tissue under large deformations, proposing a new model for fiber composite materials, laying the foundation for building white matter models by replacing geometrically wavy elements with sinusoidal oriented straight-line elements [40]. They used electron microscopy to scan the cross-sections of brainstem samples, obtaining an average axonal volume ratio of 52.7 $\pm$ 0.06 [41]. Based on this volume fraction, they established axonal components embedded in ECM as representative RVE samples, representing the smallest identifiable unit of brain white matter through particle swarm algorithm as a derivative-free optimization method, combined with finite element micromechanical simulations [41–43].

The continuous approximation of the Microstructure Model of white matter allows for the characterization of its mechanical

behavior while maintaining its connection to tissue microstructure. However, it has been observed that the fitting performance of stress-strain data is not satisfactory [44]. The Fiber-reinforced structure is a typical structure of many biological soft tissues, and scholars generally agree to use strain energy functions to simulate this behavior [45–49], supplemented by strain strengthening terms acting along the fiber direction to explain the role of axon bearing in the ECM. To characterize the directionality of the brain, it is necessary to consider introducing a vector representing the preferred direction of fibers in the calculation of the strain energy functional to achieve structured bonding. Polignon et al. initially proposed a general quadratic form with only I_4 representing anisotropy [50]. Swedberg et al. established a continuum-based hyperelastic constitutive model to describe the stress-strain relationship of tendons and ligaments under tension loads [51]. Ning et al. characterized the mechanical behavior of the brainstem as a transversely isotropic hyperelastic response [52]. The above models only have one anisotropic invariant I_4, making it impossible to predict anisotropy under small strain states. The strain energy function must depend on the pseudo-invariant I_5 [53,54]. Feng et al. demonstrated through dynamic shear testing of sheep brains that strain energy functions containing both I_4 and I_5 are essential for predicting the mechanical behavior of white matter [16,55,56]. Many scholars have introduced strain energy functions with both I_4 and I_5 anisotropic invariants to construct targeted transversely isotropic hyperelastic models for skeletal muscles [57], ligaments [46,58,59], and brain white matter [12,16,52,55,56,60]. Weiss et al. assumed the elastic response of ligaments and tendons primarily composed of collagen fibers to be isotropic matrix and the forces between collagen fiber families and their interactions [46]. Delp et al. introduced I_4 and I_5 to represent the interaction between fibers and the matrix as resistance along the fiber and transverse fibers [48].

Previous studies have provided valuable research on brain tissue from experiments to models. However, there have been fewer reports on the regional and directional effects of strain and strain rate on gray and white matter. Research quantifying the influence of axon fibers on the transverse and axial properties of the matrix through a combination of phenomenological and structural approaches is still lacking. In this study, the porcine brain was divided into regions including the brainstem, cerebellum, and cerebrum (corona radiata, corpus callosum, cortex, thalamus), and compressed to 0.3 strain under quasi-static conditions at two strain rates (high and low) and considering directionality. We systematically investigated the effects of strain rate, region, and directionality on the mechanical behavior of brain tissue. In addressing the research question, we utilized Criscione's description of transversely isotropic materials [61] and explicitly and independently represented the stresses along fiber and cross-fiber directions using the strain invariants I_1, I_4 and I_5, under the assumption of fiber loading. To our knowledge, this is the first time such a model has been introduced to characterize brain white matter. Based on the mechanical behavior of brain tissue, we determined the contributions of gray and white matter matrix and axons during loading, aiming to enhance our understanding and predictive capability of traumatic brain injury.

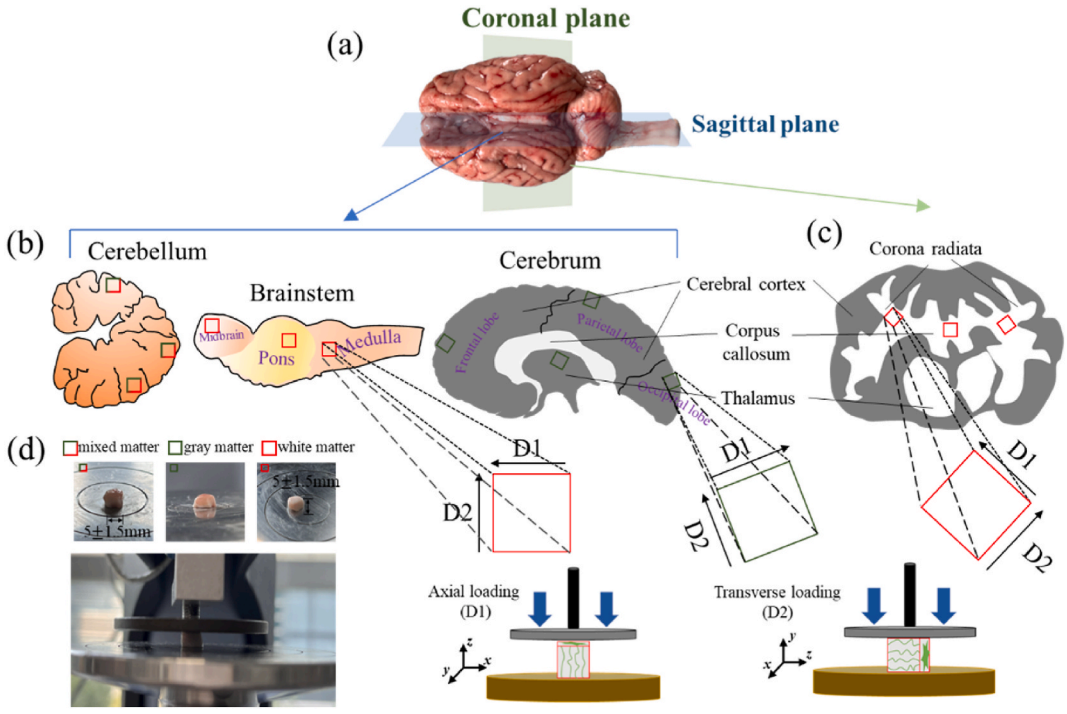

Fig. 1. (a) The fresh porcine brain is cut along (b) coronal plane (Including cerebellum, brainstem, and cerebrum) and (c) sagittal plane (d) Compression testing of white matter and schematic diagrams of axial and transverse loading.

2. Materials and methods

2.1. Specimen preparation

The pig brain tissues (N = 120) used in this study were obtained from around 8-month-old adult castrated pigs (N = 17) purchased from a local slaughterhouse within minutes after slaughter. To prevent tissue dehydration, the dissected pig brain tissues were stored in PBS solution at 4 °C until sampling. All experiments reported in this study were conducted within 6 h after the animal died.

In this study, due to the maximum thickness of the cortex, all samples were dissected as 5*5*5 mm cubes [9]. First, the soft meninges on the surface of the brain tissue were removed to explore the mechanical properties of the brain parenchyma only. The entire brain tissue was partitioned into three parts: brainstem, cerebellum, and cerebrum.

A custom surgical knife, consisting of two parallel surgical knives equipped with 23# blades with an interval spacing of 5 mm, was utilized to section the cerebrum into 5 mm-thick slices along the coronal and sagittal planes, as depicted in Fig. 1 (a). The corona radiata and corpus callosum were sampled following the direction of fibers (axial direction D1, transverse direction D2). For a sampling of the cerebral cortex and thalamus, the sections were taken perpendicular to the coronal plane for D1 and parallel to it for D2. The brainstem was separated along the descending axon by dividing it following axial (D1) and transverse (D2) directions. Samples were taken from the midbrain, pons, and medulla oblongata, as illustrated in Fig. 1(b) and (c). The cerebellum has a gray matter outer layer and a white matter inner layer with small cerebellar medullary fibers arranged in a branching pattern. However, the fiber orientation inside the white matter is not clear. Samples consisted of approximately equal amounts of white and gray matter, with D1 and D2 distinguished in the same way as the cerebral cortex.

2.2. Experimental setup

The Shimadzu testing machine (EZ-LX, Shimadzu, Japan) was used to conduct compression tests on the tissue specimen. The specimen was placed on a flat round tray. The lubricant was applied to the pressing plate and tray before placing the specimen each time to reduce the end friction effect of the specimen, which is similar to the unconfined compression test, as shown in Fig. 1 (d). To determine the mechanical properties of brain tissue under quasi-static conditions, two loading rates (shown in Table 1) were set at 0.005 mm/s and 0.5 mm/s respectively. The compression test was stopped at the strain of 0.3. This was because the present study is to obtain brain tissue properties before head injury and brain tissue could start to have compressive failure as its peak strain reaches 30 % [4].

Only load F and displacement Δx can be obtained through the sensor. The engineering stress reflects the load in compression divided by the sample section S_0, and the engineering strain reflects the material deformation except for the original length of the sample L_0. Compression results in an increase in the cross-sectional area of the sample and a decrease in the length of the sample. The brain tissue has a large elastic deformation and is almost incompressible [62–64]. Then the engineering stress and strain and the real stress and strain are transformed as

$$\sigma = \frac{\sigma_T S_0}{S} = \sigma_T(1+\varepsilon), \varepsilon = \int_{L_0}^{L} \frac{1}{L} dL = \ln(1+\varepsilon_T) \tag{1}$$

where S and L are the length and loading area during the loading deformation process, additionally,L_0 and S_0 represent the initial length and initial area σ_T and ε_T represent the engineering stress and engineering strain respectively.

3. Constitutive model

The deformation gradient tensor is expressed as $\boldsymbol{F} = \partial x/\partial X$, where x is the point in the reference configuration and X is the point in the current configuration. The corresponding left and right Cauchy–Green deformation tensors are $\boldsymbol{C} = \boldsymbol{F}^T\boldsymbol{F}, \boldsymbol{B} = \boldsymbol{F}\boldsymbol{F}^T$. The relative volume change under the two configurations is $J = \det \boldsymbol{F}$, and $\boldsymbol{F}$ is divided into the product of the dilatational part with volume-change and the distortional part with volume-preservation [65], $\boldsymbol{F} = J^{1/3}\overline{\boldsymbol{F}}, \boldsymbol{C} = J^{2/3}\overline{\boldsymbol{C}}$. $\overline{\boldsymbol{F}}$ and $\overline{\boldsymbol{C}}$ become the modified deformation gradient and the modified right Cauchy-Green deformation tensor respectively, meeting $\det\overline{\boldsymbol{F}} = \bar{\lambda}_1\bar{\lambda}_2\bar{\lambda}_3 = 1$ and $\det\overline{\boldsymbol{C}} = (\det\overline{\boldsymbol{F}})^2 = 1$. The modified

Table 1
Tested regions and sample quantity for compression tests.

Region	Cerebrum								Brainstem		Cerebellum	
	White matter				Gray matter				White matter		Mixed	
	Corona Radiata		Corpus callosum		Cerebral Cortex		Thalamus					
	D1	D2	D1	D2	D1	D2	D1	D2	D1	D2	D1	D2
$\dot{\varepsilon} = 0.001/s$	5	5	5	5	5	5	5	5	5	5	5	5
$\dot{\varepsilon} = 0.1/s$	5	5	5	5	5	5	5	5	5	5	5	5
Total qty	20		20		20		20		20		20	

principal stretches $\bar{\lambda}$ satisfies the relationship $\bar{\lambda}_i = J^{-1/3}\lambda_i (i = 1,2,3)$.

$$\bar{I}_1 = \mathrm{tr}\bar{\boldsymbol{C}}, \bar{I}_2 = \frac{1}{2}\left[(tr\bar{\boldsymbol{C}})^2 - tr\bar{\boldsymbol{C}}^2\right], \bar{I}_3 = \det\bar{\boldsymbol{C}}, \bar{I}_4 = a_0 \cdot \bar{\boldsymbol{C}}a_0, \bar{I}_5 = a_0 \cdot \bar{\boldsymbol{C}}^2 a_0 \tag{2}$$

$a_0(X)$ represents the unit vector field in the direction of the transverse isotropic axis at any point X in the reference configuration. The mechanical behavior of biological soft tissues is usually characterized by the phenomenological method based on the mechanics of continuous media or the microstructural approach to material structure. Phenomenological constitutive relation is mainly based on the fitting of data under various stress states with the assumption of isotropy, with the disadvantage that it cannot uniformly explain the load-dependent behavior exhibited by many soft tissues and lacks insight into the nature of the material. Based on histological observations, brain tissue can be divided into gray matter, which is structurally isotropic, and white matter, which exhibits anisotropy due to the presence of axonal fibers and myelin sheaths. By considering the treatment of muscle tissue by previous workers [46–48] and assuming that the white matter and its axons surrounded by myelin sheaths satisfy the continuity assumption, we propose a propriety model that takes into account the continuum media mechanics and the white matter structure can describe its deformation behavior with a strain energy density function of

$$W = W_{\mathrm{vol-c}} + W_{\mathrm{vol-p}} = W_{\mathrm{vol-c}}(J) + W_{\mathrm{iso}}(\bar{I}_1, \bar{I}_2) + W_{\mathrm{axon}}(\bar{I}_4) + W_{\mathrm{a-i}}(\bar{I}_1, \bar{I}_4, \bar{I}_5) \tag{3}$$

The strain energy function is expressed in two parts, $W_{\mathrm{vol-c}}$ and $W_{\mathrm{vol-p}}$ represent the volume change and volume preservation respectively, and $W_{\mathrm{vol-p}}$ is further refined to express the strain energy $W_{\mathrm{iso}}(\bar{I}_1, \bar{I}_2)$ of the isotropic matrix, the strain energy $W_{\mathrm{axon}}(\bar{I}_4)$ of the axon itself, and $W_{\mathrm{a-i}}(\bar{I}_1, \bar{I}_4, \bar{I}_5)$ that represents the interaction between the axon and the isotropic matrix.

3.1. Constitutive model of gray matter

Gray matter is usually considered to be isotropic [16] with an effective bulk modulus much larger than the shear modulus and almost incompressible, and the two-parameter strain energy equation proposed by Mooney to characterize rubber is widely used for elastomer deformation [66], and the same concept can be applied to gray matter to evaluate the mechanical properties of materials whose strain energy density depends on the first and second strain invariants, according to Eqs. (2) and (3), by which the strain energy W_{iso} of an isotropic matrix is expressed as follows:

$$W = W_{\mathrm{vol-c}} + W_{\mathrm{iso}} = W_{\mathrm{vol-c}}(J) + C_1(\bar{I}_1 - 3) + C_2(\bar{I}_2 - 3) \tag{4}$$

According to Eq. (4), the second kind of Piola-Kirchhoff stress (PK2) $\boldsymbol{T}$ is obtained from the strain energy density function,

$$\begin{aligned} \boldsymbol{T} &= \boldsymbol{T}_{\mathrm{vol-c}} + \boldsymbol{T}_{\mathrm{iso}} = 2\frac{\partial W}{\partial \boldsymbol{C}} = Jp\boldsymbol{C}^{-1} + J^{-2/3}\mathbb{P} : \bar{\boldsymbol{T}} \\ &= Jp\boldsymbol{C}^{-1} + 2J^{-2/3}\mathbb{P} : \frac{\partial W_{\mathrm{iso}}(\bar{\boldsymbol{C}})}{\partial \bar{\boldsymbol{C}}} \\ &= Jp\boldsymbol{C}^{-1} + 2J^{-2/3}\mathbb{P} : [(C_1 + C_2\bar{I}_1)\boldsymbol{I} - C_2\bar{\boldsymbol{C}}] \end{aligned} \tag{5}$$

where $\mathbb{P}$ is a fourth-order tensor representing the projection tensor relative to the reference configuration through the $\boldsymbol{C}$ representation. Cauchy stress tensor $\boldsymbol{\sigma}$ is defined as the second-order symmetric stress on the current configuration, and the force acting on the unit reference configuration area is the first kind of Piola-Kirchhoff stress (PK1) $\boldsymbol{P}$, which is called the nominal stress. According to the transformation relationship between the reference configuration and the current configuration, $\boldsymbol{T} = \boldsymbol{F}^{-1}\boldsymbol{P} = J\boldsymbol{F}^{-1}\boldsymbol{\sigma}\boldsymbol{F}^{-\mathrm{T}}$, and substituting into Eq. (5), it follows that,

$$\begin{aligned} \boldsymbol{\sigma} &= \frac{1}{J}\boldsymbol{F}\boldsymbol{T}\boldsymbol{F}^{\mathrm{T}} = \frac{2}{J}\boldsymbol{F}\left(\frac{\partial W_{\mathrm{vol-c}}(J)}{\partial \boldsymbol{C}} + \frac{\partial W_{\mathrm{iso}}(\bar{\boldsymbol{C}})}{\partial \boldsymbol{C}}\right)\boldsymbol{F}^{\mathrm{T}} \\ &= \frac{2}{J}\left(\boldsymbol{F}\frac{\partial W_{\mathrm{vol-c}}(J)}{\partial \boldsymbol{C}}\boldsymbol{F}^{\mathrm{T}} + J^{\frac{1}{3}}\bar{\boldsymbol{F}}J^{-2/3}\mathbb{P} : \frac{\partial W_{\mathrm{iso}}(\bar{\boldsymbol{C}})}{\partial \bar{\boldsymbol{C}}}J^{\frac{1}{3}}\bar{\boldsymbol{F}}^{\mathrm{T}}\right) \\ &= p\boldsymbol{I} + \frac{1}{J}\bar{\boldsymbol{F}}(\mathbb{P} : \bar{\boldsymbol{T}})\bar{\boldsymbol{F}}^{\mathrm{T}} \end{aligned} \tag{6}$$

When the loading direction is along the Z-axis, Eq. (6) can be simplified as follows:

$$\boldsymbol{\sigma}_{33} = 2\left(\lambda_z^2 - \lambda_z^{-1}\right)\left(C_1 + C_2\lambda_z^{-1}\right) \tag{7}$$

The engineering stress obtained from the experiment is substituted into Eq. (1). Subsequently, using Eq. (7), the material parameters C_1 and C_2 for brain gray matter are determined.

3.2. Constitutive model of white matter

We modeled the white matter as a fiber-reinforced composite with transverse isotropic material symmetry, which is similar to the previous method used to express ligaments [46], but the difference is that the fiber bundle in the ligament has no supporting effect. The multilayer sheath formed by the repeated folding and compression of myelin sheath cells around the axon in the white matter can

withstand pressure. For the additional contribution of axonal fiber, the quadratic standard enhanced strain energy function can be considered [53,54], where

$$W = W_{\text{vol-c}} + W_{\text{vol-p}} = W_{\text{vol-c}}(J) + C_1(\bar{I}_1 - 3) + C_2(\bar{I}_2 - 3) + \frac{C_3}{2}(\bar{I}_4 - 1)^2 + G_1[B_1(\bar{I}_4, \bar{I}_5)]^2 + G_2[B_2(\bar{I}_1, \bar{I}_4, \bar{I}_5)]^2 \tag{8}$$

The last two terms on the right-hand side of the equation above represent the interaction between the axon and the isotropic matrix, where G_1 and G_2 denote the effective shear modulus along the axon and the effective shear modulus perpendicular to the fiber, respectively, from which the resistance of the isotropic white matter matrix wrapped around the axon to shear along and across the axon can be obtained, the penultimate item represents the strain energy of the fiber itself, and C_3 defines the measurement method of fiber strength [52]. We quote Criscione's description of fiber-reinforced materials, using strain invariants I_1, I_4, and I_5 to explicitly and independently represent the resistance of brain white matter to along fiber shear and cross fiber shear [61]. Two new strain invariants were obtained as

$$B_1 = \sqrt{\frac{\bar{I}_5}{\bar{I}_4^2} - 1}, B_2 = \cosh^{-1}\left(\frac{\bar{I}_1\bar{I}_4 - \bar{I}_5}{2\sqrt{\bar{I}_4}}\right) = \ln\left[\left(\frac{\bar{I}_1\bar{I}_4 - \bar{I}_5}{2\sqrt{\bar{I}_4}}\right) + \sqrt{\left(\frac{\bar{I}_1\bar{I}_4 - \bar{I}_5}{2\sqrt{\bar{I}_4}}\right)^2 - 1}\right] \tag{9}$$

Then PK1 is

$$\begin{aligned} \boldsymbol{T} &= \boldsymbol{T}_{\text{vol-c}} + \boldsymbol{T}_{\text{vol-p}} = 2\frac{\partial W}{\partial \boldsymbol{C}} \\ &= 2\left(\frac{\partial W_{\text{vol-c}}}{\partial \boldsymbol{C}} + \frac{\partial W_{\text{iso}}}{\partial \boldsymbol{C}} + \frac{\partial W_{\text{axon}}}{\partial \boldsymbol{C}} + \frac{\partial W_{\text{a-i}}}{\partial \boldsymbol{C}}\right) \\ &= 2\left(\frac{\partial W_{\text{vol-c}}}{\partial J}\frac{\partial J}{\partial \boldsymbol{C}} + \frac{\partial W_{\text{iso}}}{\partial \bar{\boldsymbol{C}}}\frac{\partial \bar{\boldsymbol{C}}}{\partial \boldsymbol{C}} + \frac{\partial W_{\text{axon}}}{\partial \bar{\boldsymbol{C}}}\frac{\partial \bar{\boldsymbol{C}}}{\partial \boldsymbol{C}} + \frac{\partial W_{\text{a-i}}}{\partial \bar{\boldsymbol{C}}}\frac{\partial \bar{\boldsymbol{C}}}{\partial \boldsymbol{C}}\right) \\ &= Jp\boldsymbol{C}^{-1} + 2J^{-2/3}\mathbb{P} : \bar{\boldsymbol{T}} \end{aligned} \tag{10}$$

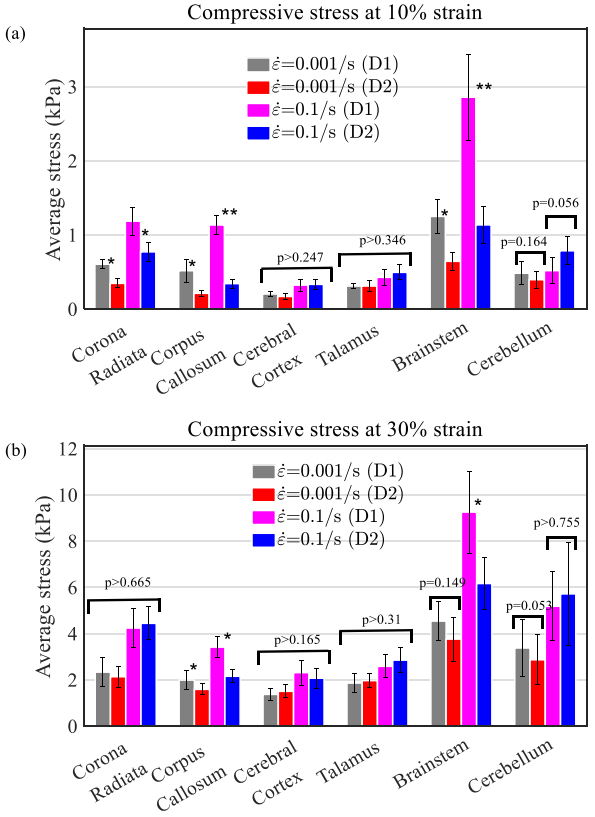

Fig. 2. Summary of direction dependency of different strain rates at strains of (a) 10 % and (b) 30 %.

By the conversion relationship between Cauchy stress and PK2, combined with Eqs. (8)–(10), when the loading direction was along the white matter axon direction,

$$\sigma = \boldsymbol{\sigma}_{33} - \boldsymbol{\sigma}_{22} = 2\left(\lambda_z^2 - \lambda_z^{-1}\right)\left(C_1 + C_2\lambda_z^{-1}\right) + 2C_3\left(\lambda_z^4 - \lambda_z^2\right) \tag{11}$$

when transverse to the axon direction (see Appendix A for the detailed derivation),

$$\sigma = \boldsymbol{\sigma}_{22} - \boldsymbol{\sigma}_{11} = 2\left[C_1 + C_2\lambda_y^{-1} - \frac{3G_2 \quad \ln(\lambda_y)\lambda_y}{1-\lambda_y^3}\right]\left(\lambda_y^2 - \lambda_y^{-1}\right) \tag{12}$$

The stress-strain relationships under axial and transverse loading of white matter are fitted using Eqs. (11) and (12) to obtain the material parameters C_1, C_2, C_3, G_2.

4. Result and discussion

Fig. 2 displays the average stress of brain tissue in two loading directions under compression strains of 10 % and 30 %. As the strain rate increases, the stiffness of the brain tissue increases, and the strain rate effect in each region is significant ($p < 0.05$), which has been confirmed by numerous scholars [8,15,17,18]. The cerebellar experimental samples are mixed materials and randomly sampled. The average stress levels of D1 and D2 alternate, and there is no statistically significant difference. Hence, there is no significance in studying their directional dependence.

Variations in loading direction and rate sensitivity arise due to regional disparities. Gray matter, composed of neuronal cell bodies and glial cells, exhibits no significant difference in D1 and D2 between the thalamus and cortical regions, indicating isotropic behavior. Since the cortex covers the surface of the entire brain, tested samples were taken from different areas (frontal, parietal, occipital, and temporal lobes). But the results showed relatively low variation. Stress-strain curves along D1 and D2 showed an interleaving pattern, even reaching near overlap in the low-strain region, as shown in Fig. 4 (a). Directionality of the thalamus during low-strain-rate loading is similar to that of the cortex. As the strain rate increases, the differences between the D1 and D2 stress-strain curves become more pronounced, but the trends remain consistent and stress statistics across the loading phase show no significant difference. These findings are supported by numerous studies [7,8,14,67]. Scholars have assessed the anisotropy of gray matter using diffusion tensor imaging (DTI) and obtained low-level anisotropy scores represented by fractional anisotropy (FA) values within the range of 0–0.4, with the thalamus slightly higher.

The composition of white matter can be simplified as a homogeneous glial cell matrix and a homogeneous nerve fiber bundle with loading direction dependence. The corpus callosum showed greater average axial stress than transverse. At a strain of 10 %, $\dot{\varepsilon} = 0.001/s$, the stiffness of D1 in the corpus callosum is 2.24 times that of D2. As the strain rate increasing to $\dot{\varepsilon} = 0.1/s$, $\overline{\sigma}_{D1}/\overline{\sigma}_{D2} = 3.30$, and when the strain increases to 30 %, the difference between the two groups increases from 1.25 times to 1.59 times as the strain rate increases. Based on Fig. 2, the same phenomenon was observed in the brainstem, where $\varepsilon = 10\%, \dot{\varepsilon} = 0.001/s, \overline{\sigma}_{D1}/\overline{\sigma}_{D2} = 1.94$ and $\dot{\varepsilon} = 0.1/s, \overline{\sigma}_{D1}/\overline{\sigma}_{D2} = 2.50$, when the strain reached 30 %, the average stress ratios obtained under the two loading rates become 1.21 and 1.50, respectively. This may be due to the presence of fiber bundles with higher Young's modulus along D1 during the loading process, resulting in a higher apparent modulus and stronger resistance to deformation. In the initial loading stage, stress increases faster compared to D2. The strain rate effect amplifies the difference in average stress between the loading directions of the corpus callosum and brainstem. However, in Fig. 2 (b), the difference in brainstem under low strain rate loading was found to be insignificant ($p = 0.15$). Unlike the easily-sampled corpus callosum, the fiber direction of the brainstem was complex. While its main direction was perpendicular to the cross-section, the fiber bundle density in the medulla oblongata, pons, and midbrain was different. Additionally, fiber bundles in other directions [14], such as the pontocerebellar tract extending perpendicular to the coronal plane, could result in an increase in stiffness in the D2 direction, making it impossible to cover the transversely isotropic nature of the brainstem due to the small sample size.

When the corona radiata is compressed to 10 % strain, the average axial stress is greater than the transverse. However, when the strain is increased to 30 %, the directional dependence of the corona radiata seems to vanish. Even under high strain rate loading, the stiffness in the transverse fiber direction is greater, although the difference is not significant. In contrast, the axial stress in the corpus callosum always surpasses the transverse stress throughout the loading process, and the stress disparity between the two directions tends to widen under high strain. Interestingly, the nonlinear characteristics of the axial stress-strain relation disappear, as depicted in Fig. 4 (b). The highly concentrated fiber axis during the compression process may be the reason for the linear elastic characteristics exhibited, ignoring the matrix contribution. However, the small sample size cannot be excluded as a possible reason. Under low strain rate loading, the corona radiata in the D1 direction is consistently greater than D2. As the strain increases, the difference between the stress curves of the two directions initially increases and then decreases, with this trend continuing even under high strain. In fact, the average stress in D2 may even surpass that in D1. Although the corona radiata is a connecting part between the central gray matter and peripheral white matter of the brain, composed of numerous non-myelinated nerve fibers that radiate towards the main axis direction (D1), it does not exhibit directional dependency. However, due to the divergent nature of fiber orientation, it is challenging to quantify the proportion of fibers deviating from the main axis in samples taken at various positions along the main axis. Any increase in the proportion of these fibers will result in an increase in the stiffness of D2 and a decrease in that of D1. Among the three regions of white matter studied, the corpus callosum demonstrates the highest degree of anisotropy. Guilfoyle et al. used diffusion tensor imaging of mixed mouse brain tissue at 7.0 T to correlate the anisotropy score (FA) with local neural structure, similarly finding that the corpus

callosum exhibits higher anisotropy [25]. Chiara Giordano quantitatively demonstrated the correlation between mechanical anisotropy and FA, indicating that the corpus callosum has FA values ranging from 0.6 to 1.0, the highest among all regions of the brain.

Ignoring the impact of loading direction, the data from ten compressions in each test area were statistically divided into six cases and compared in pairs to explore the regional effects of brain tissue. as shown in Fig. 3(a) and (b). Consistent with the views of previous studies, the brainstem is the stiffest region in brain tissue [6,10,11,18]. At $\varepsilon = 0.3, \dot{\varepsilon} = 0.001/s$, the average stress was 4.151 kPa in the brainstem and 3.121 kPa in the cerebellum, but the difference was not statistically significant ($p = 0.056$). The directional dependence of the brainstem was not significant under this condition, which may be due to the small sample size of this study. As a representative of mixed tissue, the average stress in the cerebellum was higher than that in the gray matter of the cerebrum (thalamus/cortex). However, there was no statistically significant difference in the white matter of the cerebrum (corpus callosum/corona radiata), and it was only higher than the corpus callosum at 30 % strain.

Fig. 4 (d) shows the average stress-strain curves of gray matter (thalamus/cortex) and white matter (corona radiata/corpus callosum) for a total of 20 samples at two different strain rates. The stress of white matter remains consistently higher than that of gray matter throughout the loading process. The average stress of white matter in the brain (2.010 kPa) is significantly higher than that of gray matter (1.674 kPa) when compressed to maximum strain at low strain rates ($p = 0.044$). Moreover, as the strain rate increases, the difference in stiffness between white and gray matter becomes more significant (white matter $\bar{\sigma} = 3.563$ kPa vs. gray matter $\bar{\sigma} = 2.454$ kPa, $p = 0.003$). Studies have consistently reported that white matter is greater stiffness than gray matter in bovine brain indentation experiments [19–21], human brain compression, shear, and indentation tests [8,68], micro indentation of mouse brain [67], and sheep brain shear tests [16]. Nevertheless, there are few studies that present different perspectives. Christ et al. found that the elastic modulus of gray matter in female mice is higher than that of white matter, as revealed by AFM [69], and Chatelin et al. conducted rheological tests on the corona radiata and thalamus of the human brain, which showed that there was no significant difference in stiffness between them [6]. In addition to in vitro tests, several researchers have employed magnetic resonance elastography (MRE) techniques to conduct in vivo experiments align with the findings of this study [26,28]. Nonetheless, other studies documented conflicting trends [27]. The intricate structure and dynamics of brain tissue, encompassing time, physiological state, sample size, and the methods and excitation frequencies employed to elicit the elastic properties in vitro experiments, have contributed to these discrepancies. The authors posit that the distinctions in mechanical characteristics between gray and white matter result from differences in their structure and composition. Gray matter, exhibiting a lower modulus, can decelerate external force impacts, while white matter, with a higher modulus, provides superior support and connectivity functions. The strain rate effect is more apparent in white matter than in gray matter, attributable to the presence of fiber bundles, which make the porosity more evident and vulnerable to fluid loss than gray matter. High loading rates can diminish fluid loss in white matter samples [70]. Fig. 4 (c) depicts the average stress-strain curves for ten samples from four regions of the cerebrum, ignoring directionality. The corona radiata is observed to be the region with the highest stiffness, while the corpus callosum and thalamus show nearly identical stress trend at low strain rates, but their differences are magnified as the strain rate increases, although the stress peak values seem to be similar. Despite the homogeneous gray matter within each region, regional differences still exist, with the thalamus exhibiting higher average stress than the cortex, except for high strain rate loading up to a strain of 0.3 ($p = 0.0927$), as shown in Fig. 3 (b). The hypothesis of the corona radiata as the hardest region in the brain shows significant differences for both the cortex and thalamus in all four cases, except for no significant difference in peak stress at low strain rates ($p = 0.154$), as demonstrated in Fig. 3 (a). As mentioned earlier, distinguishing between the stiffness of the corpus callosum and thalamus is difficult. The corpus callosum, as white matter, is slightly harder than the cortex at low strains ($p = 0.057$), which becomes more significant at high strains ($p = 0.045$).

Some studies found that the initial shear modulus of the porcine thalamus is higher than that of the cortex through shear tests, and satisfied the relationship $\mu_T > \mu_{CR} > \mu_C > \mu_{CC}$. Additionally, it has been observed that the thalamus was stiffer than the cortex, but the corpus callosum was the softest of the four [7,71]. In this study, the stiffness difference between the corpus callosum and cortex will increase with the increase of strain rate. Hence, it is reasonable to attribute the variation in in loading rate and loading mode causes the stiffness difference in different regions. Jin et al. suggested that the stiffness of corona radiata under compression loading is the largest,

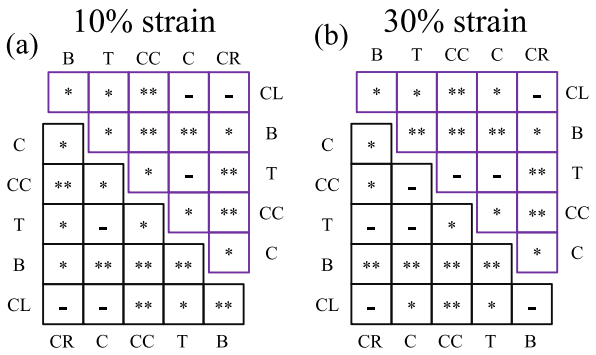

Fig. 3. Compression test results for significant difference between brain regions at strains of (a) 10 % and (b) 30 %. CR = Corona radiata, CC = Corpus callosum, C= Cerebral cortex, T = Thalamus, B = Brainstem, CL = Cerebellum. '-', '*' and '**' represent no significant differences, with significance levels of 0.1 and 0.001, respectively. Black bottom table = strain rate: 0.1/s, purple top table = strain rate: 0.001/s.

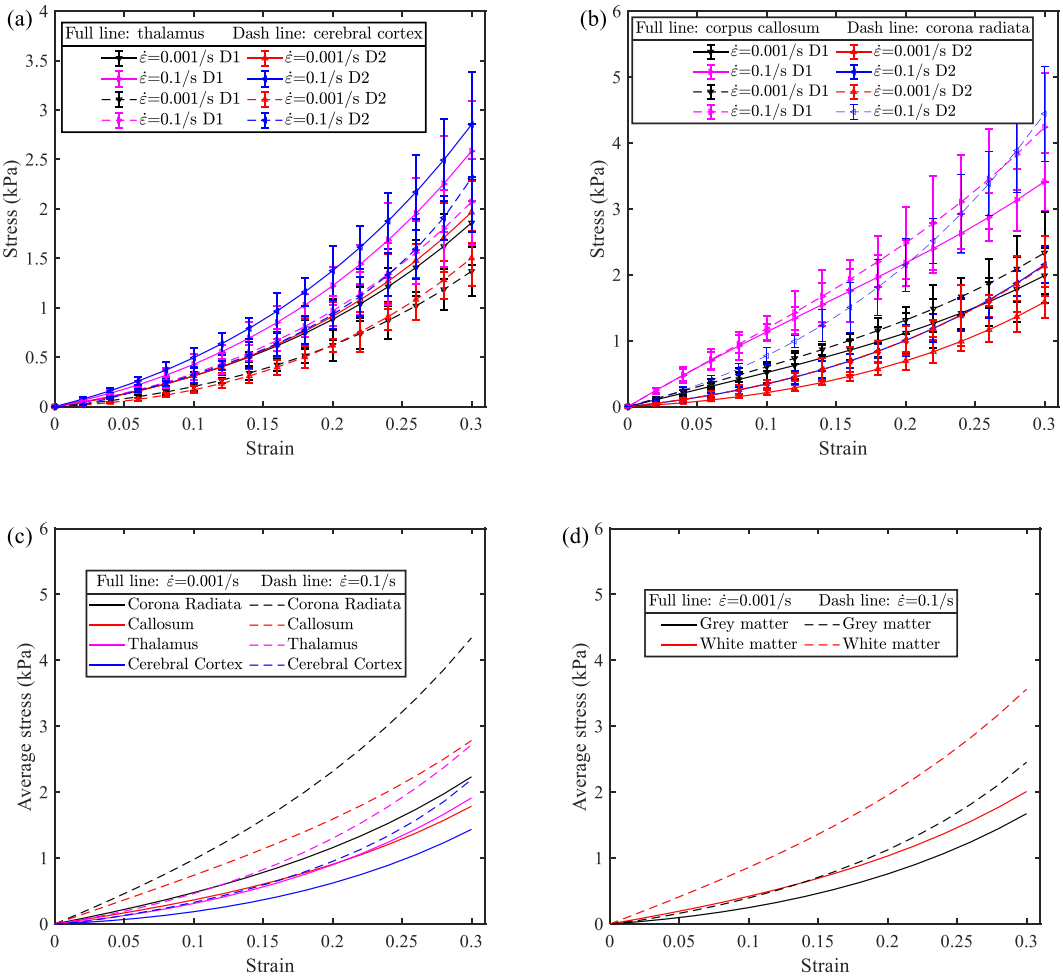

Fig. 4. Stress-strain curves of (a) thalamus and cerebral cortex and (b) corpus callosum and corona radiata. Average stress-strain curves of (c) four non-directional cerebral regions and (d) cerebral gray and white matter.

Table 2
(a) Apparent elastic modulus of brain tissue strain rate of $\dot{\varepsilon} = 0.001/s$. (b) Apparent elastic modulus of brain tissue strain rate of $\dot{\varepsilon} = 0.1/s$.

Apparent elastic moduli	E_1 (0–0.1)	E_2 (0–0.2)	E_3 (0–0.3)
Corona radiata	4.755	6.822	10.752
Corpus callosum	3.645	5.408	8.818
Cerebral cortex	1.863	4.341	8.148
Thalamus	3.103	5.870	10.150
Brainstem	9.464	12.754	19.287
Cerebellum	4.393	9.485	17.329
Apparent elastic moduli	E_1 (0–0.1)	E_2 (0–0.2)	E_3 (0–0.3)
Corona radiata	9.783	13.353	20.279
Corpus callosum	7.382	8.524	11.928
Cerebral cortex	3.278	6.216	12.413
Thalamus	4.612	8.374	14.193
Brainstem	19.959	23.846	33.294
Cerebellum	6.518	16.406	31.565

which is consistent with our research [8]. Holzapfel and other researchers found in the compression test of the human brain that the stiffness of the cerebral cortex is greater than that of the white matter, and the corpus callosum is the softest [9]. However, their use of indentation experiments has yielded contrasting results [72]. It is speculated that the influence of the meninges and the prolonged death time (within 60 h of the test death) may be considered. Li et al. reveals the cortex, thalamus, corona radiata, and corpus callosum sections of the cerebrum did not significantly differ between strains of 0.25 and 0.5 [18]. Nonetheless, magnetic imaging technology revealed that the corpus callosum is stiffer than the corona radiata [26]. Interestingly, the results of different studies on the regional dependency of brain tissue properties are always contradictory, largely depending on the loading mode, even for the simplest uniaxial loading modes of tension and compression. Table 2 presents the apparent moduli E_1, E_2, and E_3 for stress-strain responses obtained for strain ranges of 0–0.1 (0–10 %), 0.1–0.2 (10–20 %), and 0.2–0.3 (20–30 %), respectively. We observed that with increasing strain rate, the apparent elastic modulus also increased, further confirming the strain rate effect. The positive correlation between the apparent elastic modulus and strain indicates that brain tissue has compressive strain-strengthening properties, and some studies have shown that it is negatively correlated with strain during tension, with compressive stress greater than tensile stress at the same absolute value of strain [8,9,18,52]. While both brain tissue and muscle tissue are modeled as transverse isotropic bodies, muscle fibers will buckle under compression, whereas axons can resist compression. Some researchers suggest that at the microstructural level, the cerebrospinal fluid in cells and extracellular matrix offers substantial resistance to

Compression, but limited resistance to tension [2], whereas others propose that the compression-resistant attribute of brain tissue arises from the squeezing of the cell bodies [13].

Through the established constitutive model, the elastic response of the white matter was assumed to be the glial cell matrix, axon fibers, and the resistance of their interaction, and the average stress-strain of different regions of brain tissue under two strain rates were fitted, as shown in Table 3. The model demonstrates an excellent fit to the mechanical behavior of brain tissue ($0.971<R^2<0.999$), quantitatively exploring the role of fiber bundles in the compression process. Assuming the brain tissue is incompressible, the initial shear modulus of the matrix is $\mu_0 = 2(C_1 + C_2)$, and the Poisson's ratio is 0.5, furthermore, the initial Young's modulus satisfies $E_0 = 3\mu_0$. The strength of the corona radiata, corpus callosum, and brainstem fibers relative to the matrix's Young's modulus at low strain rates was 1.140, 1.912, and 0.706, respectively. The corpus callosum had the highest proportion, and the fibers were highly oriented. At high strain rates, this value decreased to 0.802, 1.258, and 0.857, respectively, all to varying degrees, and the effect of strain rate was more evident in the matrix than in the fibers. Arbogast et al. predicted that the stiffness of fibers was three times that of the matrix through the created structural mathematical model [73]. In addition, studies have indicated that axons are 10 times that of isotropic matrices [52,74]. Recently, Jamal et al. conducted AFM indentation experiments to measure the ratio of axons to matrix in the corpus callosum and corona radiata of sheep brain, which were 1.892 and 1.728, respectively, which seems to be closer to our results. It is almost impossible to measure the stress in fibers through in vitro experiments. Although no consistent quantitative results have been obtained, qualitatively it is believed that the fiber stress in white matter cannot be ignored, and the assumption of isotropy is not valid. Young's modulus of the thalamus is higher than that of the corpus callosum and the corona radiata matrix, which seems to explain to some extent the contradictory regional dependence results of different scholars. When collecting samples of white matter in the brain, the distribution of axons is somewhat random. If the sample size is small and the fiber density is insufficient, the measured hardness of gray matter may be higher than that of white matter. Even in the highly oriented corpus callosum, there may still be biased axons, which can affect test results. Additionally, the regional trend may depend on the length scale. As shown in Table 3, the cross-fiber shear modulus is highest in the corona radiata, followed by the brainstem, and lowest in the corpus callosum. These fitting parameters are obtained under transverse loading, which supports our observation that the corona radiata has the most biased axons, while the corpus callosum has the strongest axonal orientation.

Table 3
(a) Material parameters at the strain rate of $\dot{\varepsilon} = 0.001/s$. (b) Material parameters at strain rate of $\dot{\varepsilon} = 0.1/s$.

	Corona Radiata	Corpus callosum	Cerebral Cortex	Thalamus	Brainstem	Cerebellum
C_1	−1.565	−1.455	−1.284	−1.247	−2.338	−2.536
C_2	1.742	1.559	1.434	1.586	2.892	2.939
C_3	1.246	1.193			2.346	
G_2	0.2126	0.084			0.1842	
μ_0	0.3540	0.1880	0.30	0.6780	1.1080	0.8060
E_0	1.0932	0.5640	1.2000	2.0340	3.3240	2.4180
$R^2_{(D1)}$	0.9972	0.9889	0.9959	0.9999	0.9932	0.9965
$R^2_{(D2)}$	0.9863	0.9759			0.9821	0.9710
	Corona Radiata	Corpus callosum	Cerebral Cortex	Thalamus	Brainstem	Cerebellum
C_1	−2.261	−1.486	−1.7085	−1.623	−3.273	−5.291
C_2	2.743	1.832	1.9985	2.15	4.739	5.7360
C_3	2.329	2.632			5.384	
G_2	0.5808	0.021			0.1576	
μ_0	0.9640	0.6920	0.58	1.0540	2.0940	0.89
E_0	2.8920	2.0760	1.74	3.1620	6.2820	2.67
$R^2_{(D1)}$	0.9867	0.9795	0.9892	0.9996	0.9904	0.9868
$R^2_{(D2)}$	0.9851	0.9714			0.9878	0.9804

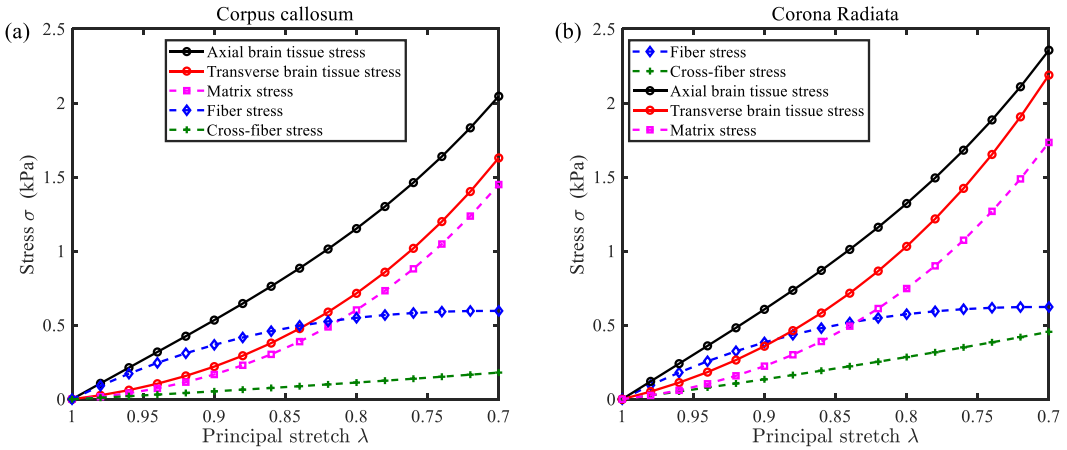

Fig. 5. Predicted stress-strain curve by model for fiber, matrix, and cross-fiber in compression, (a) corpus callosum (b) corona radiata.

Fig. 5 depicts the brain tissue, axonal fibers, and inter-fiber stresses of the corpus callosum and corona radiata as a function of the principal stretch, using fitting parameters obtained under low strain rate. Specifically, Fig. 5 (a) illustrates that during the initial stage of shortening of the corpus callosum under the principal stretch (D1), the fiber stress (represented by the blue solid line) dominates, whereas as the stretch decreases, the matrix stress (indicated by the purple dashed line) dominates. This phenomenon arises from the fact that the axonal fiber bundle experiences stress exceeding the critical value during compression, and the fibers underneath the bundle fail to attain adequate symmetry in shape and initial state, therefore, some fibers within the bundle lose stability abruptly, resulting in the collapse and deformation of the entire bundle. The mechanical mechanism presented above explains the previously mentioned phenomenon, i.e., the increase in strain leading to the weakening of the difference between axial and transverse directions of the white matter. Moreover, Arbogast et al. achieved a higher fiber-to-matrix stiffness ratio than in this study (30 % strain) at smaller deformations (2.5 % strain), providing a cross-study comparison. The corpus callosum has a high density of axonal fibers that are highly oriented relative to the corona radiata, as illustrated in Fig. 5 (b). In this state, the critical point of matrix fiber stress alternation is more deformed than that of the corona radiata, and the overall fiber bundle stress is also high, satisfying $\lambda_C = 0.84 < \lambda_{CR} = 0.89$ and $\sigma_C = 0.496$ kPa $< \sigma_{CR} = 0.435$ kPa. When the strain rate increases to $\dot{\varepsilon} = 0.1/\text{s}$, the principal stretch and fiber stress at the critical point respectively become $\lambda_C = 0.77, \lambda_{CR} = 0.84$ and $\sigma_C = 1.253$ kPa, $\sigma_{CR} = 0.967$ kPa. Generally, the stress threshold for material compression rod instability is lower at high strain rates than at low strain rates. However, both the degree of deformation and fiber stress at the critical point increase. This anomalous phenomenon may originate from the physiological structure of the white matter where the fiber bundle is wrapped by the matrix providing resistance to transverse deformation under axial loading. Additionally, the presence of fiber bundles in white matter creates a porous structure [43,73], and the increase in strain rate reduces water loss rate, resulting in higher stiffness.

When the principal stretch varies in the transverse direction, the cross-fiber stress of the corpus callosum and the corona radiata is relatively small, mainly borne by the matrix surrounding the axon. The peak cross-fiber stress of the corpus callosum and the corona radiata is approximately 0.180 kPa and 0.455 kPa, respectively, with a slightly higher proportion in the corona radiata (0.208). However, at a strain rate of 0.1/s, the stresses become 0.045 and 1.243, respectively. The axonal fibers have low resistance to

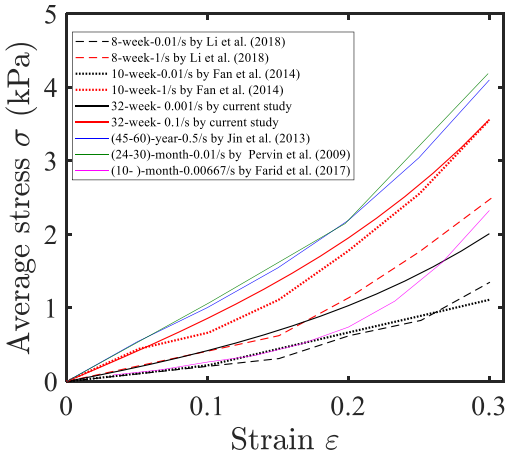

Fig. 6. Comparison of white matter compression characteristics between current study and literature.

transverse compression, and the interaction between the fibers and the matrix also has a relatively small effect on resistance. As previously mentioned, the directionality of the corona radiata is difficult to determine at $\dot{\varepsilon} = 0.1/\mathrm{s}$. Moreover, the cross-fiber stress is abnormally high, which may be the result of the structural off-axis fiber resistance being miscalculated calculated as cross-fiber stress, which is unavoidable in the transverse isotropic model. To address this issue, an anisotropic finite elastic material model with multiple fiber families may be established, and the fiber directions should be determined during sampling to obtain unit vectors in the reference configuration of the *n*th fiber.

Fig. 6 shows the statistically averaged stress-strain curves for pig brains (black and red lines), bovine brains (green solid line) [15], sheep brains (purple solid line) [17], and human brains (blue solid line) [8] as reported by previous studies. Rodents such as rats and mice were excluded from the statistics since their brain structure, which lacks gyri and sulci, differs significantly from that of large mammals and Fig. 6 ignores the differences and specific regions of the test samples and compares the measurement methods (compression), species, age, and loading rates roughly (only the mean value is not statistically significant). The stress differences between adult pigs and piglets confirm that brain tissue stiffens during development. Qualitative similarities between adult cattle and adults, as well as between pediatric porcine and lambs, seem to exist. There are indeed differences in brain tissue stress among different species, but overall, they are on the same order of magnitude, indicating that using these mammals as substitutes for human brain research is feasible.

In summary, the differences in the mechanical behavior of brain tissue are mainly reflected in age, location, type, and fiber direction. In addition to these intrinsic factors of brain tissue, sample size, hydration, loading mode, loading rate, and maximum strain also affect test results.

Previous studies have elucidated the experimental findings of this study at the microstructural level. Through MRI imaging and color-coded fiber orientation, it has been demonstrated that the gray matter appears relatively homogeneous, while fiber orientations in the corpus callosum and brainstem white matter are highly directional, with axial stresses exceeding lateral loads [14]. Histological staining of adult brainstem tissue sections revealed prominently longitudinal-oriented axon fiber bundles with compact arrangement and minimal matrix [73]. Diffusion tensor imaging (DTI) assessment of fiber orientation in coronal planes revealed radiating fibers of the corona radiata [9], which reflects insignificant differences in axial and lateral stresses in terms of mechanical behavior. At the macroscopic to mesoscopic levels of tissue histology, single axon fibers are surrounded by a one-layer thick myelin sheath, constituting the majority of the brain's white matter tissue. Micro-needle experiments, controlling axial [75] and lateral [76] deformations to detect the stiffness of single axons, revealed the contribution of fiber bundles to overall mechanical response. Furthermore, positive correlations were found between myelin content and hardness, and negative correlations were observed between protein polysaccharide content and hardness. Using histological staining methods, a negative correlation between cell count and hardness, a positive correlation between myelin content and hardness, and a negative correlation between protein polysaccharide content and hardness were revealed [77]. The higher proportion of phospholipids in white matter resulted in greater stiffness compared to gray matter. Yousefsani et al. determined the mechanical properties using analytical solutions for the uniform response of white matter structures in axial and lateral directions, then considered the deformation of the matrix and axons separately by randomly distributing the axons within the matrix [74]. Some scholars have incorporated mechanical parameters measuring fiber dispersion levels into models using the fractional anisotropy (FA) scores of brain tissue assessed through DTI [78]. Finite element analysis can help elucidate how these components interact and contribute to overall response, as well as conduct sensitivity analyses to assess the relative importance of different microstructural parameters. The presence of axonal fibers also influences the overall stiffness and strength of white matter tissue. Their distribution and arrangement determine, to some extent, the overall stiffness of the tissue, and their contribution is significant. Understanding and considering the role of axonal fibers under compression loading can help us better understand the mechanical properties of white matter tissue. The experimental results and theoretical predictions of this study provide valuable information for better understanding the mechanical properties of brain tissue and thus the structure and function of the brain. However, there are certain limitations.

Firstly, the model does not consider the time-dependent viscoelastic effects and poroelastic effects exhibited by soft tissues. The next step could involve subjecting brain tissue to Ramp-Hold loading to obtain time-varying stiffness moduli or dynamic frequency loading to obtain the complex modulus, combined with the model established in this study, to establish a Hyper-viscoelastic Model characterizing the mechanical behavior of brain tissue through consistency assessment. Secondly, the loading rates in this study fall within the quasi-static range, making it difficult to capture the short-term memory response of brain tissue under high strain rate loading. The next direction is to construct a Visco-hyperelastic Model by combining viscous dissipative potential functions using the principle of Boltzmann superposition to capture the mechanical behavior of brain tissue within a large strain rate range. Additionally, our study investigates the mechanical behavior of brain tissue under compression loading, while further exploration of other loading modes (such as tension, shear, and combined loading) remains to be explored. Furthermore, due to the ultra-soft and highly hydrated nature of brain tissue, despite efforts to minimize errors, the samples in the experimental process still cannot uniformly expand, which may affect the accuracy and reliability of our data assessment. Lastly, while large mammals serve as feasible substitutes for human brains qualitatively, quantitatively establishing their relationship remains challenging. Future experiments on human brains are still required.

5. Conclusion

This study established a constitutive model for brain tissue and derived fitting equations based on the loading direction of gray and white matter, compressing the cerebrum (cortex, thalamus, corona radiata, and corpus callosum), cerebellum, and brainstem at low and high strain rates under quasi-static constraints up to 30 % strain. The findings reveal the following.

- The heterogeneity of gray matter structures in the same region does not lead to anisotropic mechanical behavior, although even regional differences still exist. As off-fibers exist in the corona radiata, the direction dependence of the corona radiata cannot be reflected by the peak stress. The oblique angles of fibers at distinct locations are divergent, thereby underscoring the apparent anisotropy of white matter. Given the highly oriented nature of corpus callosum fibers, they exhibit the most prominent transverse isotropy.
- Conversely, an increase in strain reduces the directional dependence of white matter, whereas an increase in strain rate enhances this phenomenon. The brainstem is the stiffest among brain tissues, corona radiata is the hardest in the brain, and the cortex is the softest, with no significant difference in strength between thalamus and corpus callosum. Overall, white matter is stiffer than gray matter and the increase of strain and strain rate enhances the regional effect. Furthermore, brain tissue exhibits the characteristic of strain-stiffening behavior.
- The established model predicts that the modulus of the gray matrix is higher than that of the white matrix, and the modulus of axonal fibers is 0.802–1.912 times that of the white matter matrix. As axial loading increases the strain, the axonal fibers underwent buckling instability, and the fiber stress decreased, weakening the difference between axial and transverse stress peaks. During transverse loading, the matrix played the main resistance role. This also indicates that the damage to axons caused by axial impact on brain tissue is greater than that caused by lateral impact.

Data availability statement

The full data generated or analysed to support the conclusion during this study are included in this published article.

CRediT authorship contribution statement

Wei Kang: Writing – review & editing, Writing – original draft, Software, Methodology, Formal analysis, Data curation. **Qiao Li:** Writing – review & editing, Writing – original draft, Formal analysis, Data curation. **Lizhen Wang:** Writing – review & editing, Writing – original draft, Funding acquisition, Data curation. **Yu Zhang:** Investigation, Data curation. **Peng Xu:** Software, Resources, Data curation. **Yubo Fan:** Writing – review & editing, Resources, Project administration, Funding acquisition, Data curation.

Declaration of competing interest

There is no conflict of interest to be declared by the authors.

Acknowledgments

This work was supported by the National Natural Science Foundation of China [U2241273, 12425209], Beijing Municipal Natural Science Foundation [Z240017], the 111 project [B13003] and the Fundamental Research Funds for the Central Universities, the China Scholarship Council, the Academic Excellence Foundation of BUAA for PhD Students.

Appendix B. Supplementary data

Supplementary data to this article can be found online at https://doi.org/10.1016/j.heliyon.2024.e37979.

Appendix A. Constitutive equations

According to Eq. (3), the second-order tensor of PK2 of the volume-preserving distortion part of gray matter is written as a matrix,

$$\overline{\boldsymbol{T}} = 2\begin{bmatrix} C_1 + C_2\bar{I}_1 - C_2\boldsymbol{C}_{11} & -C_2\boldsymbol{C}_{12} & -C_2\boldsymbol{C}_{13} \\ -C_2\boldsymbol{C}_{21} & C_1 + C_2\bar{I}_1 - C_2\boldsymbol{C}_{22} & -C_2\boldsymbol{C}_{23} \\ -C_2\boldsymbol{C}_{31} & -C_2\boldsymbol{C}_{32} & C_1 + C_2\bar{I}_1 - C_2\boldsymbol{C}_{33} \end{bmatrix} \tag{A.1}$$

Assuming compression loading experiment along Z-axis, the deformation gradient tensor $\boldsymbol{F}$ and the right Cauchy Green tensor $\boldsymbol{C}$ are

$$\overline{\boldsymbol{F}} = \begin{bmatrix} \lambda_x & 0 & 0 \\ 0 & \lambda_y & 0 \\ 0 & 0 & \lambda_z \end{bmatrix}, \overline{\boldsymbol{C}} = \begin{bmatrix} \lambda_x^2 & 0 & 0 \\ 0 & \lambda_y^2 & 0 \\ 0 & 0 & \lambda_z^2 \end{bmatrix} \tag{A.2}$$

Take (A.2) into Eq (4) to obtain the Cauchy stress tensor, and assuming incompressibility and uniform deformation, the principal stretches in the x-axis and y-axis directions content $\lambda_x = \lambda_y = \lambda_z^{-\frac{1}{2}}$.

$$\boldsymbol{\sigma}=\begin{bmatrix} 2C_1\lambda_z^{-1}-2C_2\lambda_z & & \\ & 2C_1\lambda_z^{-1}-2C_2\lambda_z & \\ & & 2C_1\lambda_z^{2}-2C_2\lambda_z^{-2} \end{bmatrix}-(2C_2\bar{I}_2-p)\boldsymbol{I} \tag{A.3}$$

According to the experiment,

$$\begin{aligned} &\boldsymbol{\sigma}_{33}=\sigma \\ &\boldsymbol{\sigma}_{11}=\boldsymbol{\sigma}_{22}=0 \end{aligned} \tag{A.4}$$

then the stress is

$$\begin{aligned} \sigma=\boldsymbol{\sigma}_{33}-\boldsymbol{\sigma}_{22}&=2\left[C_1\left(\lambda_z^2-\lambda_z^{-1}\right)+C_2\left(\lambda_z-\lambda_z^{-2}\right)\right] \\ &=2\left(\lambda_z^2-\lambda_z^{-1}\right)\left(C_1+C_2\lambda_z^{-1}\right) \end{aligned} \tag{A.5}$$

The gray matter material parameters C_1 and C_2 can be obtained by bringing in the experimental data.
According to Eq. (9), the second-order tensor of PK2 of the volume-preserving distortion part of white matter is written as a matrix,

$$\begin{aligned} &\overline{\boldsymbol{T}}=2\begin{bmatrix} n-C_2\overline{\boldsymbol{C}}_{11} & -C_2\overline{\boldsymbol{C}}_{12} & -C_2\overline{\boldsymbol{C}}_{13} \\ -C_2\overline{\boldsymbol{C}}_{21} & n-C_2\overline{\boldsymbol{C}}_{22} & -C_2\overline{\boldsymbol{C}}_{23} \\ -C_2\overline{\boldsymbol{C}}_{31} & -C_2\overline{\boldsymbol{C}}_{32} & \frac{1}{2}\overline{\boldsymbol{T}}_{33} \end{bmatrix} \\ &l=\sqrt{\frac{\left(\bar{I}_5-\bar{I}_1\bar{I}_4\right)^2}{4\quad\bar{I}_4}-1}, m=\frac{\bar{I}_5-\bar{I}_1\quad\bar{I}_4}{2\quad\sqrt{\bar{I}_4}}, n=\left(C_1+C_2\bar{I}_1+\frac{G_2\quad\ln(l-m)\quad\left(\sqrt{\bar{I}_4}-\frac{\bar{I}_5-\bar{I}_1\quad\bar{I}_4}{2l}\right)}{(l-m)}\right) \\ &\overline{\boldsymbol{T}}_{33}=2\mathrm{n}-2C_2\overline{\boldsymbol{C}}_{33}+2\left[C_3(\bar{I}_4-1)+\frac{G_2\ln(l-m)\quad\left(ml+\bar{I}_1\sqrt{\bar{I}_4}l-m^2-m\bar{I}_1\sqrt{\bar{I}_4}\right)}{(l-m)\bar{I}_4 l}-\frac{2\quad\bar{I}_5G_1}{\bar{I}_4^3}\right] \\ &+\frac{4\overline{\boldsymbol{C}}_{33}\left[G_1\quad l-\bar{I}_4^{3/2}G_2\quad\ln(l-m)\right]}{\bar{I}_4^2\quad\cdot l} \end{aligned} \tag{A.6}$$

When the white matter is assumed to be incompressible and loaded along the axon direction, the isotropic plane is perpendicular to the transverse isotropic axis, satisfying $\lambda_x=\lambda_y=\lambda_z^{-\frac{1}{2}}$, $\overline{\boldsymbol{T}}$ reduced to

$$\overline{\boldsymbol{T}}=2\begin{bmatrix} C_1+C_2\left(\lambda_z^{-1}+\lambda_z^2\right) & 0 & 0 \\ 0 & C_1+C_2\left(\lambda_z^{-1}+\lambda_z^2\right) & 0 \\ 0 & 0 & C_1+C_2\lambda_z^{-1}+\left(C_3\lambda_z^2-2\lambda_z G_1\right) \end{bmatrix} \tag{A.7}$$

Cauchy stress is

$$\boldsymbol{\sigma}=\begin{bmatrix} 2\lambda_z^{-1}\left[C_1+C_2\left(\lambda_z^{-1}+\lambda_z^2\right)\right] & 0 & 0 \\ 0 & 2\lambda_z^{-1}\left[C_1+C_2\left(\lambda_z^{-1}+\lambda_z^2\right)\right] & 0 \\ 0 & 0 & 2\lambda_z^2\left[C_1+C_2\lambda_z^{-1}+\left(C_3\lambda_z^2-2\lambda_z G_1\right)\right] \end{bmatrix}-p\boldsymbol{I} \tag{A.8}$$

then the stress is

$$\sigma=\boldsymbol{\sigma}_{33}-\boldsymbol{\sigma}_{22}=2\left(\lambda_z^2-\lambda_z^{-1}\right)\left(C_1+C_2\lambda_z^{-1}\right)+2C_3\left(\lambda_z^4-\lambda_z^2\right) \tag{A.9}$$

According to Eq. (A.6), when the uniaxial load is applied transversely to the fiber direction (loading direction: y), then $\lambda_x=\left(\lambda_y\lambda_z\right)^{-1}$, $\overline{\boldsymbol{T}}$ is

$$\overline{\boldsymbol{T}} = 2\begin{bmatrix} n - C_2\overline{C}_{11} & 0 & 0 \\ 0 & n - C_2\overline{C}_{22} & 0 \\ 0 & 0 & 2n - 2C_2\overline{C}_{33} + 2C_3\left(\lambda_z^2 - 1\right) + 2\left[G_2 \ln(l-m) \quad \left(m + \bar{I}_1\sqrt{\bar{I}_4} - 2\bar{I}_4^{3/2}\right)\right]\Big/\lambda_z^2 l \end{bmatrix}$$
$$l = \sqrt{\frac{\left(\lambda_y^4\lambda_z^2 - 1\right)^2}{4 \quad \lambda_y^4 \quad \lambda_z^2}}, m = -\frac{\lambda_y^4\lambda_z^2 + 1}{2\lambda_y^2\lambda_z}, \tag{A.10}$$
$$n = \left(C_1 + C_2\bar{I}_1 + G_2 \quad \ln(l-m) \quad \left(\sqrt{\bar{I}_4} - \frac{\bar{I}_5 - \bar{I}_1 \quad \bar{I}_4}{2l}\right)(l-m)^{-1}\right)$$

Furthermore, Cauchy stress is obtained as

$$\boldsymbol{\sigma} = \overline{\boldsymbol{F}\boldsymbol{T}\boldsymbol{F}}^{\mathrm{T}} - p\boldsymbol{I} \tag{A.11}$$

The stresses on the three principal axes are

$$\begin{aligned}
\boldsymbol{\sigma}_{11} &= 2\left(\lambda_y\lambda_z\right)^{-2}\left[C_1 + C_2\left(\lambda_y^2 + \lambda_z^2\right) + G_2 \quad \ln(l-m) \quad \left(\sqrt{\bar{I}_4} - \frac{\bar{I}_5 - \bar{I}_1 \quad \bar{I}_4}{2l}\right)(l-m)^{-1}\right] - p \\
\boldsymbol{\sigma}_{22} &= 2\lambda_y^2\left\{C_1 + C_2\left[\left(\lambda_y\lambda_z\right)^{-2} + \lambda_z^2\right] + G_2 \quad \ln(l-m) \quad \left(\sqrt{\bar{I}_4} - \frac{\bar{I}_5 - \bar{I}_1 \quad \bar{I}_4}{2l}\right)(l-m)^{-1}\right\} - p \\
\boldsymbol{\sigma}_{33} &= 2\lambda_z^2\left\{\begin{array}{l} C_1 + C_2\left[\left(\lambda_y\lambda_z\right)^{-2} + \lambda_y^2\right] - G_2 \quad \lambda_z \ln(l-m)\left(\dfrac{m^2}{\sqrt{m^2-1}} - m\right) + \\ C_3\left(\lambda_z^2 - 1\right) + \dfrac{G_2 \ln(l-m) \quad \left(m + \bar{I}_1\sqrt{\bar{I}_4} - 2\lambda_z^3\right)}{\lambda_z^2 l} \end{array}\right\} - p
\end{aligned} \tag{A.12}$$

then the stress is

$$\begin{aligned}
\sigma &= \boldsymbol{\sigma}_{22} - \boldsymbol{\sigma}_{33} \\
\boldsymbol{\sigma}_{11} &= 0
\end{aligned} \tag{A.13}$$

According to our thinking, we need to eliminate the hydrostatic pressure by subtracting the stress in the x direction from the stress in the y direction, and then consider that there is no stress in the x and z directions, so, λ_z is expressed by λ_y. When the relationship between λ_z and λ_y is introduced into the first formula of Eq. (A.14), the stress-strain relationship is obtained. However, the elongation in the x and z directions is highly coupled, and without some assumptions, the analytical solution is almost impossible to obtain. We adopt the Lin approach, $\lambda_x = \lambda_z = \lambda_y^{-\frac{1}{2}}$, and we will further simplify Eq. (A.13) as,

$$\begin{aligned}
\boldsymbol{\sigma}_{11} &= 2\lambda_y^{-1}\left[C_1 + C_2\left(\lambda_y^{-1} + \lambda_y^2\right) - \frac{3G_2 \quad \ln\left(\lambda_y\right)\lambda_y}{1 - \lambda_y^3}\right] - p \\
\boldsymbol{\sigma}_{22} &= 2\lambda_y^2\left[C_1 + 2C_2\lambda_y^{-1} - \frac{3G_2 \quad \ln\left(\lambda_y\right)\lambda_y}{1 - \lambda_y^3}\right] - p \\
\boldsymbol{\sigma}_{33} &= 2\lambda_y^{-1}\left\{C_1 + C_2\left(\lambda_y^{-1} + \lambda_y^2\right) + C_3\left(\lambda_y^{-1} - 1\right) + \frac{3G_2 \quad \ln\left(\lambda_y\right)\lambda_y\left(1 - 2\lambda_y^3\right)}{1 - \lambda_y^3}\right\} - p
\end{aligned} \tag{A.14}$$

Combined with Eq. (A.14), the stress is

$$\sigma = \boldsymbol{\sigma}_{22} - \boldsymbol{\sigma}_{11} = 2\left[C_1 + C_2\lambda_y^{-1} - \frac{3G_2 \quad \ln\left(\lambda_y\right)\lambda_y}{1 - \lambda_y^3}\right]\left(\lambda_y^2 - \lambda_y^{-1}\right) \tag{A.15}$$

References

[1] R. de Rooij, E. Kuhl, Constitutive modeling of brain tissue: current perspectives, Appl. Mech. Rev. 68 (2016).

[2] S. Budday, T.C. Ovaert, G.A. Holzapfel, P. Steinmann, E. Kuhl, Fifty shades of brain: a review on the mechanical testing and modeling of brain tissue, Arch. Comput. Methods Eng. 27 (2020) 1187–1230.

[3] J. Faber, J. Hinrichsen, A. Greiner, N. Reiter, S. Budday, Tissue-scale biomechanical testing of brain tissue for the calibration of nonlinear material models, Current Protocols 2 (2022) e381.
[4] K. Miller, Biomechanics of the Brain, Springer, 2011.
[5] W. Kang, L. Wang, Y. Fan, Viscoelastic response of gray matter and white matter brain tissues under creep and relaxation, J. Biomech. 162 (2024) 111888.
[6] S. Chatelin, J. Vappou, S. Roth, J.S. Raul, R. Willinger, Towards child versus adult brain mechanical properties, J. Mech. Behav. Biomed. Mater. 6 (2012) 166–173.
[7] M.T. Prange, S.S. Margulies, Regional, directional, and age-dependent properties of the brain undergoing large deformation, J. Biomech. Eng. 124 (2002) 244–252.
[8] X. Jin, F. Zhu, H. Mao, M. Shen, K.H. Yang, A comprehensive experimental study on material properties of human brain tissue, J. Biomech. 46 (2013) 2795–2801.
[9] S. Budday, G. Sommer, C. Birkl, C. Langkammer, J. Haybaeck, J. Kohnert, M. Bauer, F. Paulsen, P. Steinmann, E. Kuhl, Mechanical characterization of human brain tissue, Acta Biomater. 48 (2017) 319–340.
[10] K.B. Arbogast, S.S. Margulies, Regional differences in mechanical properties of the porcine central nervous system, SAE Trans. (1997) 3807–3814.
[11] K.B. Arbogast, S.S. Margulies, Material characterization of the brainstem from oscillatory shear tests, J. Biomech. 31 (1998) 801–807.
[12] F. Velardi, F. Fraternali, M. Angelillo, Anisotropic constitutive equations and experimental tensile behavior of brain tissue, Biomech. Model. Mechanobiol. 5 (2006) 53–61.
[13] F. Eskandari, M. Shafieian, M.M. Aghdam, K. Laksari, Tension strain-softening and compression strain-stiffening behavior of brain white matter, Ann. Biomed. Eng. 49 (2021) 276–286.
[14] F. Eskandari, M. Shafieian, M.M. Aghdam, K. Laksari, Structural anisotropy vs. mechanical anisotropy: the contribution of axonal fibers to the material properties of brain white matter, Ann. Biomed. Eng. 49 (2021) 991–999.
[15] F. Pervin, W.W. Chen, Dynamic mechanical response of bovine gray matter and white matter brain tissues under compression, J. Biomech. 42 (2009) 731–735.
[16] Y. Feng, R.J. Okamoto, R. Namani, G.M. Genin, P.V. Bayly, Measurements of mechanical anisotropy in brain tissue and implications for transversely isotropic material models of white matter, Journal of the mechanical behavior of biomedical materials 23 (2013) 117–132.
[17] M. Hosseini Farid, A. Eslaminejad, M. Ziejewski, G. Karami, A Study on the Effects of Strain Rates on Characteristics of Brain Tissue, ASME International Mechanical Engineering Congress and Exposition, American Society of Mechanical Engineers, 2017 V003T004A003.
[18] Z. Li, H. Yang, G. Wang, X. Han, S. Zhang, Compressive properties and constitutive modeling of different regions of 8-week-old pediatric porcine brain under large strain and wide strain rates, Journal of the mechanical behavior of biomedical materials 89 (2019) 122–131.
[19] S. Budday, R. Nay, R. de Rooij, P. Steinmann, T. Wyrobek, T.C. Ovaert, E. Kuhl, Mechanical properties of gray and white matter brain tissue by indentation, J. Mech. Behav. Biomed. Mater. 46 (2015) 318–330.
[20] J. Van Dommelen, T. Van der Sande, M. Hrapko, G. Peters, Mechanical properties of brain tissue by indentation: interregional variation, Journal of the mechanical behavior of biomedical materials 3 (2010) 158–166.
[21] J. Weickenmeier, R. de Rooij, S. Budday, P. Steinmann, T.C. Ovaert, E. Kuhl, Brain stiffness increases with myelin content, Acta Biomater. 42 (2016) 265–272.
[22] B.S. Elkin, A. Ilankova, B. Morrison, Dynamic, regional mechanical properties of the porcine brain: indentation in the coronal plane, J. Biomech. Eng. 133 (2011) 071009.
[23] F. Chen, J. Zhou, Y. Li, Y. Wang, L. Li, H. Yue, Mechanical properties of porcine brain tissue in the coronal plane: interregional variations of the corona radiata, Ann. Biomed. Eng. 43 (2015) 2903–2910.
[24] A. Jamal, A. Bernardini, D. Dini, Microscale characterisation of the time-dependent mechanical behaviour of brain white matter, J. Mech. Behav. Biomed. Mater. 125 (2022) 104917.
[25] D.N. Guilfoyle, J.A. Helpern, K.O. Lim, Diffusion tensor imaging in fixed brain tissue at 7.0 T, NMR in Biomedicine, An International Journal Devoted to the Development and Application of Magnetic Resonance In Vivo 16 (2003) 77–81.
[26] C.L. Johnson, M.D. McGarry, A.A. Gharibans, J.B. Weaver, K.D. Paulsen, H. Wang, W.C. Olivero, B.P. Sutton, J.G. Georgiadis, Local mechanical properties of white matter structures in the human brain, Neuroimage 79 (2013) 145–152.
[27] M.A. Green, L.E. Bilston, R. Sinkus, In vivo brain viscoelastic properties measured by magnetic resonance elastography, NMR Biomed.: An International Journal Devoted to the Development and Application of Magnetic Resonance In vivo 21 (2008) 755–764.
[28] S.A. Kruse, G.H. Rose, K.J. Glaser, A. Manduca, J.P. Felmlee, C.R. Jack Jr., R.L. Ehman, Magnetic resonance elastography of the brain, Neuroimage 39 (2008) 231–237.
[29] L.A. Mihai, L. Chin, P.A. Janmey, A. Goriely, A comparison of hyperelastic constitutive models applicable to brain and fat tissues, J. R. Soc. Interface 12 (2015) 20150486.
[30] L.A. Mihai, S. Budday, G.A. Holzapfel, E. Kuhl, A. Goriely, A family of hyperelastic models for human brain tissue, J. Mech. Phys. Solid. 106 (2017) 60–79.
[31] T. Kaster, I. Sack, A. Samani, Measurement of the hyperelastic properties of ex vivo brain tissue slices, J. Biomech. 44 (2011) 1158–1163.
[32] Y. Pan, L. Iorga, A.A. Pelegri, Numerical generation of a random chopped fiber composite RVE and its elastic properties, Compos. Sci. Technol. 68 (2008) 2792–2798.
[33] Y. Pan, D.I. Shreiber, A.A. Pelegri, A transition model for finite element simulation of kinematics of central nervous system white matter, IEEE Trans. Biomed. Eng. 58 (2011) 3443–3446.
[34] Y. Pan, D. Sullivan, D.I. Shreiber, A.A. Pelegri, Finite element modeling of CNS white matter kinematics: use of a 3D RVE to determine material properties, Front. Bioeng. Biotechnol. 1 (2013) 19.
[35] X. Wu, J.G. Georgiadis, A.A. Pelegri, Harmonic viscoelastic response of 3D histology-informed white matter model, Mol. Cell. Neurosci. 123 (2022) 103782.
[36] X. Wu, J.G. Georgiadis, A.A. Pelegri, Brain white matter model of orthotropic viscoelastic properties in frequency domain, in: ASME International Mechanical Engineering Congress and Exposition, American Society of Mechanical Engineers, 2019 V003T004A024.
[37] M. Agarwal, P. Pasupathy, A.A. Pelegri, Oligodendrocyte tethering effect on hyperelastic 3D response of axons in white matter, J. Mech. Behav. Biomed. Mater. 134 (2022) 105394.
[38] M. Agarwal, A.A. Pelegri, Hyper-viscoelastic 3D response of axons subjected to repeated tensile loads in brain white matter, in: ASME International Mechanical Engineering Congress and Exposition, American Society of Mechanical Engineers, 2022 V004T005A046.
[39] M. Agarwal, A.A. Pelegri, An Ogden hyperelastic 3D micromechanical model to depict Poynting effect in brain white matter, Heliyon (2024) e25379.
[40] G. Karami, M. Garnich, Effective moduli and failure considerations for composites with periodic fiber waviness, Compos. Struct. 67 (2005) 461–475.
[41] S. Javid, A. Rezaei, G. Karami, A micromechanical procedure for viscoelastic characterization of the axons and ECM of the brainstem, Journal of the mechanical behavior of biomedical materials 30 (2014) 290–299.
[42] G. Karami, N. Grundman, N. Abolfathi, A. Naik, M. Ziejewski, A micromechanical hyperelastic modeling of brain white matter under large deformation, Journal of the mechanical behavior of biomedical materials 2 (2009) 243–254.
[43] N. Abolfathi, A. Naik, M. Sotudeh Chafi, G. Karami, M. Ziejewski, A micromechanical procedure for modelling the anisotropic mechanical properties of brain white matter, Comput. Methods Biomech. Biomed. Eng. 12 (2009) 249–262.
[44] D.F. Meaney, Relationship between structural modeling and hyperelastic material behavior: application to CNS white matter, Biomech. Model. Mechanobiol. 1 (2003) 279–293.
[45] J. Humphrey, F. Yin, On constitutive relations and finite deformations of passive cardiac tissue: I. A pseudostrain-energy function (1987).
[46] J.A. Weiss, B.N. Maker, S. Govindjee, Finite element implementation of incompressible, transversely isotropic hyperelasticity, Comput. Methods Appl. Mech. Eng. 135 (1996) 107–128.
[47] J.A. Weiss, J.C. Gardiner, Computational modeling of ligament mechanics, Critical Reviews™ in Biomedical Engineering 29 (2001).
[48] S.S. Blemker, P.M. Pinsky, S.L. Delp, A 3D model of muscle reveals the causes of nonuniform strains in the biceps brachii, J. Biomech. 38 (2005) 657–665.

[49] X. Ning, Q. Zhu, Y. Lanir, S.S. Margulies, A transversely isotropic viscoelastic constitutive equation for brainstem undergoing finite deformation, J. Biomech. Eng. 128 (2006) 925–933.
[50] D.A. Polignone, C.O. Horgan, Cavitation for incompressible anisotropic nonlinearly elastic spheres, J. Elasticity 33 (1993) 27–65.
[51] A.M. Swedberg, S.P. Reese, S.A. Maas, B.J. Ellis, J.A. Weiss, Continuum description of the Poisson′ s ratio of ligament and tendon under finite deformation, J. Biomech. 47 (2014) 3201–3209.
[52] X. Ning, Q. Zhu, Y. Lanir, S.S. Margulies, A transversely isotropic viscoelastic constitutive equation for brainstem undergoing finite deformation (2006).
[53] J. Merodio, R. Ogden, Instabilities and loss of ellipticity in fiber-reinforced compressible non-linearly elastic solids under plane deformation, Int. J. Solid Struct. 40 (2003) 4707–4727.
[54] J. Merodio, R. Ogden, Mechanical response of fiber-reinforced incompressible non-linearly elastic solids, Int. J. Non Lin. Mech. 40 (2005) 213–227.
[55] Y. Feng, S. Qiu, X. Xia, S. Ji, C.-H. Lee, A computational study of invariant I5 in a nearly incompressible transversely isotropic model for white matter, J. Biomech. 57 (2017) 146–151.
[56] Y. Feng, R.J. Okamoto, G.M. Genin, P.V. Bayly, On the accuracy and fitting of transversely isotropic material models, journal of the mechanical behavior of biomedical materials 61 (2016) 554–566.
[57] D.A. Morrow, T.L.H. Donahue, G.M. Odegard, K.R. Kaufman, Transversely isotropic tensile material properties of skeletal muscle tissue, Journal of the mechanical behavior of biomedical materials 3 (2010) 124–129.
[58] S. Thomopoulos, G.M. Genin, Tendon and Ligament Biomechanics, Orthopaedic Biomechanics, 2012, p. 49.
[59] S.P. Lake, K.S. Miller, D.M. Elliott, L.J. Soslowsky, Tensile properties and fiber alignment of human supraspinatus tendon in the transverse direction demonstrate inhomogeneity, nonlinearity, and regional isotropy, J. Biomech. 43 (2010) 727–732.
[60] S. Chatelin, C. Deck, R. Willinger, An anisotropic viscous hyperelastic constitutive law for brain material finite-element modeling, Journal of Biorheology 27 (2012) 26–37.
[61] J.C. Criscione, A.S. Douglas, W.C. Hunter, Physically based strain invariant set for materials exhibiting transversely isotropic behavior, J. Mech. Phys. Solid. 49 (2001) 871–897.
[62] W. Kang, P. Xu, Y. Yue, L. Wang, Y. Fan, Difference analysis of phenomenological models with two variable forms for soft tissue quasi-static mechanical characterization, Comput. Biol. Med. (2022) 106150.
[63] K. Wei, X. Peng, B. Weiping, Y. Yanxian, W. Lizhen, F. Yubo, Mechanical testing of biological soft tissue and related theoretical research, Acta Armamentarii 43 (2022) 2164.
[64] W. Kang, Y. Zhang, W. Bu, Y. Zhao, L. Wang, S. Liu, Statistical analysis of mechanical properties of biological soft tissue under quasi-static mechanical loading, Medicine in Novel Technology and Devices 17 (2023) 100202.
[65] G.A. Holzapfel, T.C. Gasser, R.W. Ogden, A new constitutive framework for arterial wall mechanics and a comparative study of material models, Journal of elasticity and the physical science of solids 61 (2000) 1–48.
[66] M. Mooney, A theory of large elastic deformation, J. Appl. Phys. 11 (1940) 582–592.
[67] D.B. MacManus, B. Pierrat, J.G. Murphy, M.D. Gilchrist, Region and species dependent mechanical properties of adolescent and young adult brain tissue, Sci. Rep. 7 (2017) 13729.
[68] J.D. Finan, S.N. Sundaresh, B.S. Elkin, G.M. McKhann II, B. Morrison III, Regional mechanical properties of human brain tissue for computational models of traumatic brain injury, Acta Biomater. 55 (2017) 333–339.
[69] A.F. Christ, K. Franze, H. Gautier, P. Moshayedi, J. Fawcett, R.J. Franklin, R.T. Karadottir, J. Guck, Mechanical difference between white and gray matter in the rat cerebellum measured by scanning force microscopy, J. Biomech. 43 (2010) 2986–2992.
[70] S. Budday, G. Sommer, J. Haybaeck, P. Steinmann, G.A. Holzapfel, E. Kuhl, Rheological characterization of human brain tissue, Acta Biomater. 60 (2017) 315–329.
[71] B. Coats, S.S. Margulies, Material properties of porcine parietal cortex, J. Biomech. 39 (2006) 2521–2525.
[72] S. Budday, R. Nay, R. de Rooij, P. Steinmann, T. Wyrobek, T.C. Ovaert, E. Kuhl, Mechanical properties of gray and white matter brain tissue by indentation, Journal of the mechanical behavior of biomedical materials 46 (2015) 318–330.
[73] K.B. Arbogast, S.S. Margulies, A fiber-reinforced composite model of the viscoelastic behavior of the brainstem in shear, J. Biomech. 32 (1999) 865–870.
[74] S.A. Yousefsani, A. Shamloo, F. Farahmand, Nonlinear mechanics of soft composites: hyperelastic characterization of white matter tissue components, Biomech. Model. Mechanobiol. 19 (2020) 1143–1153.
[75] D.E. Ingber, S.R. Heidemann, P. Lamoureux, R.E. Buxbaum, Opposing views on tensegrity as a structural framework for understanding cell mechanics, J. Appl. Physiol. 89 (2000) 1663–1678.
[76] R. Bernal, P.A. Pullarkat, F. Melo, Mechanical properties of axons, Phys. Rev. Lett. 99 (2007) 018301.
[77] S. Budday, M. Sarem, L. Starck, G. Sommer, J. Pfefferle, N. Phunchago, E. Kuhl, F. Paulsen, P. Steinmann, V. Shastri, Towards microstructure-informed material models for human brain tissue, Acta Biomater. 104 (2020) 53–65.
[78] C. Giordano, S. Kleiven, Connecting fractional anisotropy from medical images with mechanical anisotropy of a hyperviscoelastic fibre-reinforced constitutive model for brain tissue, Journal of the Royal Society Interface 11 (2014) 20130914.